25th ABCM International Congress of Mechanical Engineering
October 20-25, 2019, Uberlândia, MG, Brazil

COB-2019-0330
MATHEMATICAL MODEL FOR HYDROGEN PRODUCTION IN A SOLAR THERMOCHEMICAL REACTOR VIA STEAM REFORMING OF TOLUENE

Maria C. Souza
Emerson B. dos Anjos
Polytechnic school – UPE, Laboratory of Enviromental and Energetic Technology; Street Benfica – 455, Madalena, Recife – PE, Brazil.
Mcs3@poli.br
emersonanjos@poli.br

Cláudio C. B. Oliveira
Department of Chemical Engineering , Federal University of Penambuco (UFPE), phone (81) 2126-8901, R Prof Artur de Sá, 50740-521, Rceife – PE, Brazil.
claudiothor@hotmail.com

Jornandes D. Silva
Polytechnic school – UPE, Laboratory of Enviromental and Energetic Technology; Street Benfica – 455, Madalena, Recife – PE, Brazil.
jornandesdias@poli.br

Abstract. *The heat and mass transfer performances of the steam reforming of toluene (SRT) in a solar thermochemical reactor (STR) were numerically investigated. A mathematical model is developed to simulate the heat and mass transfer processes coupled with thermochemical reaction kinetic in STR with radiative loss. The effect of several parameters including the superficial velocity (V_{sg}), operating time (t_i) and operating temperature (top.) were investigated. As results, when the V_{sg} is increased, the temperature profiles of the gas phase are remarkably decreasing. The reactant mole concentration (C_7H_8 and H_2O) distributions decrease sharply along the STR length. On the other hand, product mole concentration distributions increase remarkably along the STR length. According to simulated results, the overall conversions of C_7H_8 reach the maximum value of 94.58% at the operating time of 3.0 hours. The Dimensionless Flow Rate (DFR) of (H_2 and CO) products is remarkably increased with the operating temperature and the maximum values of H_2 and CO can be achieved 1.6521, 0.2548 at 1250k.*

Keywords: *Mass transfer, Heat transfer, Mathematical model, Hydrogen.*

1. INTRODUCTION

With the continuing growth in the world's population, living standards, and economy, energy demand is also increasing significantly, not only resulting in the sharp depletion of fossil fuels but also inducing serious environmental problems, such as global warming and air pollution (Wang et al., 2019). The issues of fossil fuel depletion and climate change have resulted in development of solar industrial process solutions. Reforming system which makes use of solar heat to drive high temperature endothermic chemical reactions are known as solar thermochemical processes (Dolan et al., 2016). The solar reforming system typically contains two main components: a solar concentrator and a chemical reactor. The incoming solar radiation is collected and reflected by the concentrator, forming a highly intense radiative flux on the aperture of reactor. The concentrated solar radiation penetrates into the reactor and is directly absorbed, causing a gradual temperature rise. High-temperature foam skeleton transfers the heat to the feed reactants and facilitates the endothermic chemical reaction (Chen et al., 2018).

As an emerging energy technology, solar driven steam reforming of toluene (SRT) can be considered as a promising process for producing solar hydrogen (H_2). Hydrogen is able to store energy from primary sources then it is an important energy vector. In particular, it is the most desirable energy carriers due to its cleanness and zero emissions property. Furthermore, hydrogen is consumed in fuel cells, achieving an electrical efficiency higher than 90% and it is going to have an important role inside the suitable energy supply chain (Leonzio et al., 2019). STR is an important and valuable device for reforming process where many applications can be carried out at high operating temperature. The modelling of STRs is still an open issue, thus the topic is a very actual subject for renewable energy engineering

(Ceylan et al., 2017). Usually, physical and chemical parameters are simultaneously coupled in the mathematical model through the fluid-solid mass transfer, fluid-solid heat transfer, momentum transfer and chemical reactions processes (Chen et al., 2018). In this context, mathematical models are efficiently used as tool to analyze the reactor design and operating conditions from STR behavior.

In this work, a mathematical model has been developed to investigate the heat and mass transfer phenomena coupled with thermochemical reaction kinetics in STR. The performance from STR using the SRT process is numerically investigated in terms of the temperature profiles in the gaseous phase. In addition, the reactant and product distributions, effect of the operating time on the overall conversions of toluene, and the dimensionless flow rate (DFR) of H_2 relative to initial concentration of toluene, respectively.

2. KINETIC MECHANISM

In this study, the SRT reaction was considered as follows.

$$C_7H_8 + 7H_2O \leftrightarrow 7CO + 11H_2\,;\ \Delta H^0_{298K} = +869.10\,kJ/mol \tag{1a}$$

The component models of these reactions are defined as toluene (C_7H_8), water (H_2O), hydrogen (H_2), carbon and monoxide (CO).

2.1 THERMOCHEMICAL MODELLING

2.1.1. Kinetic model

The global rate from Eq. (1a) is defined as:

$$R_{SRT} = k_r\, C_{C_7H_8}\,;\ k_r = k_{r,0}\, exp\left(\frac{E_a}{RT_g}\right) \tag{1b}$$

Where R_{SRT} (kmol/kg_{cat} sec) is the global reaction rate, k_r (m^3/kg_{cat} s) is the constant of the global reaction rate (Eq (1)), C_{C7H8} (kmol/m^3) is the concentration of toluene, respectively; $k_{r,0}$ (m^3/kg_{cat} s) is the frequency factor, E_a (kJ/kmol) is the activation energy, R (kJ/kmol K) is the universal gas constant, T_g (K) is the gas phase respectively.

The net rates of each chemical component (r_i, i = CH_4, H_2O, CO and H_2) are computed in Table 1 and can be found in Reference (Cruz and Silva, 2017).

Table 1. Net rates of components i from Eq (1).

Components	Equations of net rates	Components	Equations of net rates
C_7H_8	$r_{C_7H_8} = -\eta_1 R_{SRT}$	CO	$r_{CO} = +7\eta_1 R_{SRT}$
H_2O	$r_{H_2O} = -7\eta_1 R_{SRT}$	H_2	$r_{H_2} = +11\eta_1 R_{SRT}$

2.1.2. Thermochemical process

In the last two decades, researches have proven the efficient use of solar thermal energy for driving highly endothermic reforming reactions. For this purpose, a schematic setup (see Figure. 1) was employed to study the SRT process in SRT.

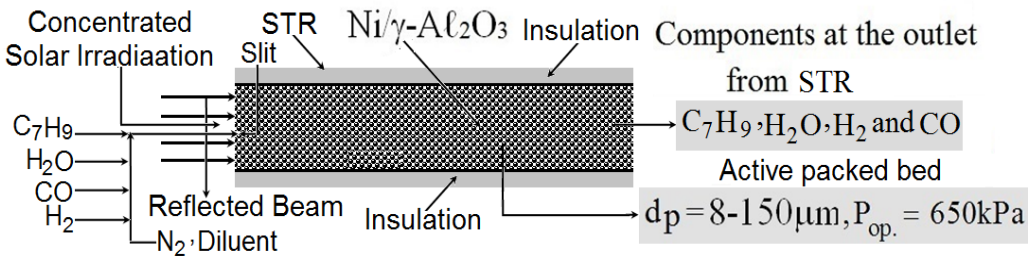

Figure 1. schematic setup from STR

2.2 STR modelling

The main purpose of this section is the development of a precise mathematical model that will be able to simulate the behavior of the SRT processing system. To evaluate the key variables of the developed mathematical modelling, we adopt the following assumptions: (i) ideal gas phase, (ii) axial dispersion inside from STR, (iii) no diffusion phenomena of chemical components at the catalyst surface and inside the catalyst occur, (iv) constant STR pressure (no pressure drop in the STR) and constant superficial velocity, (v) STR operates under dynamic regime, (v) porosity in the axial direction from SRT was considered constant, (vi) constant physical properties (density, catalyst weight, uniform particle sizes) over the range of operating conditions from SRT, respectively. Based on the above assumptions, the energy and mass equations (inside from SRT) are formulated as follows.

-Energy balance in the gas phase

$$\sum_{i=1}^{4}\rho_i C_{p,i}\frac{\partial T_g}{\partial t}+\frac{4q_g}{\pi d_c^2}\sum_{i=1}^{4}\rho_i C_{p,i}\frac{\partial T_g}{\partial z_j}=\left(\lambda_g\left(T_g\right)+\frac{16\,n^2\sigma T_\infty^3}{3k_R}\right)\frac{\partial^2 T_g}{\partial z_j^2}+h_{gs}\frac{\left(1-\varepsilon_b\right)}{\varepsilon_b}\frac{3}{R_p}\left(T_g-T_s\big|_{r=R_p}\right)+\Delta H_1\,\eta_1 R_{SRT} \tag{2a}$$

In the Eq(2a), ρ_i (kg/m^3) is the density of gaseous mixture, T_g (K) is the temperature of the gaseous phase, $C_{p,I}$ (kJ/kg k) is the molar heat capacity at constant pressure of the gaseous mixture, λ_g (W/m K) is the gas thermal conductivity, n (-) is the refractive index, σ (W/m^2 T^4) is the Stefan–Boltzmann constant, T_∞ (K) is the ambient temperature, k_R (m^{-1}) is the Rosseland extinction coefficient in porous medium, h_{gs} (W/m^2 K) is the gas-solid heat transfer coefficient, ε_b (m^{3}gas/ m^{3}reactor) is the void fraction of bed, r_p (m) is the particle radius, T_s (K) is the temperature of the solid phase, ΔH_1 (kJ/kmol) is the heat of reaction, η_1 (-) is the effectiveness factor from Eq(1), respectively.

The suitable initial and boundary conditions from Eq (2a) are given as follows

-Initial conditions, i.e., t = 0; the inlet face surface from STR, i.e., Z = 0$^+$; at the outlet face surface from ST-μPB reactor, i.e., z = L_z;

$$T_g\big|_{t=0,0\le z\le L_z}=0;\ \lambda_g\left(T_g\right)\frac{\partial T_g}{\partial z_j}\bigg|_{z=0^+,t\ge 0}=\frac{4q_g}{\pi d_c^2}\sum_{i=1}^{4}\rho_i C_{p,i}\left(T_g\big|_{z=0^+,t\ge 0}-T_{g,in}\right);\ \frac{\partial T_g}{\partial z_j}\bigg|_{z=L_z,t\ge 0}=0 \tag{2b}$$

-Mass balance of components i (i = C_7H_8, H_2O, H_2, CO) in STR

$$\frac{\partial C_i}{\partial t}+\frac{4q_g}{\pi d_c^2}\frac{\partial C_i}{\partial z_j}=D_{ax,i}\frac{\partial^2 C_i}{\partial z_j^2}+\frac{\left(1-\varepsilon_b\right)}{\varepsilon_b}\eta_1\sum_{i=1}^{4}\rho_i r_i;0\le z\le L_z,t>0 \tag{3a}$$

In Eq(3a), C_i (kmol/m^3) is the concentration of components i in the gas phase, q_g (m^3/s) is the gas flow rate, d_c (m) is the inner diameter from STR, $D_{ax,j}$ (m^2/s) is the axial mass dispersion coefficient of components i, r_i (kmol/kg$_{cat.}$ s) is the net rates from components i, respectively.

The suitable initial and boundary conditions from Eq (3a) are reported as follows.

-Initial condition, .i.e., t = 0; at the inlet face from ST-μPB reactor, i.e., Z = 0$^+$; at the outlet face from ST-μPB reactor, i.e., Z = L_z;

$$C_i\big|_{t=0,0\le z\le L_z}=0;\varepsilon_b D_{ax,i}\frac{\partial C_i}{\partial z_j}\bigg|_{z=0^+,t\ge 0}=\frac{4q_g}{\pi d_c^2}\left(C_i\big|_{z=0^+,t\ge 0}-C_{i,in}\right);\ \frac{\partial C_i}{\partial z_j}\bigg|_{z=L_z,t\ge 0}=0 \tag{3b}$$

2.3 Application of the Laplace transform

The Laplace transform of unknown functions ($T_g(Z_j,t)$ and $C_i(Z_j,t)$, $t \ge 0$) is defined by the integrals (if they exist) from "Eqs(5a)-(5c)"and these equations can be found in Ref. (Silva et al., 2019). On the other hand, the Laplace transform of the time derivate from partial differential (PD) equations is given by "Eq(5d)-(5f)" and these equations are also met in Ref. (Silva et al., 2019). Thus, Eqs(2a)-(3b) were transformed to ordinary differential equations (ODEs) in together with their prescribed initial and boundary conditions. As results, transformed equations are reported as follows.

- Energy balance for the gas phase in the Laplace domain;

$$\lambda_g\left(T_g\right)+\frac{16\,n^2\,\sigma T_\infty^3}{3k_R}\frac{d^2\bar{T}_g\left(z_j,s_k\right)}{dz_j^2}-\frac{4q_g}{\pi d_c^2}\sum_{i=1}^{4}\rho_i C_{p,i}\frac{d\bar{T}_g\left(z_j,s_k\right)}{dz_j}+\left(h_{gs}\frac{\left(1-\varepsilon_b\right)}{\varepsilon_b}\frac{3}{R_p}-s_k\sum_{i=1}^{4}\rho_i C_{p,i}\right)$$
$$\bar{T}_g\left(z_j,s_k\right)-h_{gs}\frac{\left(1-\varepsilon_b\right)}{\varepsilon_b}\frac{3}{R_p}\bar{T}_s\left(z_j,s_k\right)\Big|_{r=R_p}=0 \tag{4a}$$

The boundary conditions from Eq(4a) are transformed in the Laplace domain as follows.

$$\frac{d\bar{T}_g\left(z_j,s_k\right)}{dz_j}\Big|_{z_j=0^+,s_k\geq 0}=\frac{4q_g\sum_{i=1}^{4}\rho_i C_{p,i}}{\pi d_c^2\,\lambda_g\left(\bar{T}_g\right)}\left(\bar{T}_g\left(z_j,s_k\right)\Big|_{z_j=0^+,s_k\geq 0}-\frac{\bar{T}_g\left(z_j\right)}{s_k}\right);\ \frac{d\bar{T}_g\left(z_j,s_k\right)}{dz_j}\Big|_{z_j=L_z,s_k\geq 0}=0 \tag{4b}$$

-Mass balance of chemical components i in the Laplace domain;

$$D_{ax,i}\frac{d^2\bar{C}_i\left(z_j,s_k\right)}{dz_j^2}-\frac{4q_g}{\pi d_c^2}\frac{d\bar{C}_i\left(z_j,s_k\right)}{dz_j}-s_k\bar{C}_i\left(z_j,s_k\right)+\frac{\left(1-\varepsilon_b\right)}{\varepsilon_b}\eta_1\sum_{i=1}^{4}\bar{r}_i\left(z_j,s_k\right)=0 \tag{5a}$$

The boundary conditions from Eq(4a) are shown in the Laplace domain as follows.

$$\varepsilon_b D_{ax,i}\frac{d\bar{C}_i\left(z_j,s_k\right)}{dz_j}\Big|_{z_j=0^+,s_k\geq 0}=\frac{4q_g}{\pi d_c^2}\left(\bar{C}_i\left(z_j,s_k\right)\Big|_{z_j=0^+,s_k\geq 0}-\frac{\bar{C}_i\left(z_j\right)}{s_k}\right);\ \frac{d\bar{C}_i\left(z_j,s_k\right)}{dz_j}\Big|_{z_j=L_z,s_k\geq 0}=0 \tag{5b}$$

2.3.1. Numerical solution of transformed equations

The mathematical difficulties for solving a system of nonlinear ordinary differential equations are great due to the numerical stability. In view that, some numerical methods have been used to investigate numerical solutions. The selection of numerical method is dependent on the desired accuracy as well as concerns about the stability and robustness of the system while maintaining computational efficiency (Silva, 2015). In this study, the system of the transformed equations (Eqs(4a)-(5b)) in jointly with the boundary conditions are discretized by finite volume (FV) method. After the discretization from the transformed equations using VF method, the inverse Laplace transformation is applied (Teles and Silva, 2015). The trapezoidal method was used to approximate the transformed functions in time domain and details can found in Ref. (Silva and Oliveira, 2012). It is found that the variation of integration step has negligible influence on the results obtained of this work. Therefore, an integration step of 10^{-6} was used to reach all the simulated results in this article.

3. RESULTS AND DISCUSSIONS

3.1. Parameters for the simulation

A computational algorithm using the FORTRAN 95 was elaborated by authors to solve the model equations mentioned in this work. Therefore, operating conditions, kinetic parameters, energy parameters, mass parameters for simulating the SRT process variables are presented in table 2. As results, some physical parameters are defined as function of the operating temperature. Thus, these physical parameters were obtained at the operating temperature of the SRT process.

Table 2. Operating conditions, kinetic parameters and mass parameters.

Categories	Properties	Numerical Values
Operation Conditions	Operating pressure (atm) Operating temperature (K) Gas flow rate (m^3/s) Reactor diameter (d_c) Reactor length (m)	1.01 1800 $3.5x10^{-5}$ -$5.5x10^{-5}$ 0.032 0.14
Kinetic parameters	Activation Energy (kJ/kmol K) Universal Constant of gases (m^3atm/kmol K) Frequency Factor (m^3/kg_{cat} s)	196 8.314 $2.26x10^{13}$
Energy parameters	Density of the gaseous mixture (kg/m^3) Molar heat capacity of the gaseous mixture ((kJ/kg K) STR diameter (mm) Gas thermal conductivity (W/m K) Stefan-Boltzmann constant ($W/m^2 T^4$) Ambient temperature (T_∞, K) Rosseland extinction coefficient (m^{-1})	0.793 1.079 0.40 109.123 $2.67x10^{-8}$ 300 $1.738x10^4$
Mass parameters	Initial concentration of C_7H_8 ($kmol/m^3$) Initial concentration of H_2O ($kmol/m^3$) Initial concentration of H_2 ($kmol/m^3$) Initial concentration of CO ($kmol/m^3$) Axial mass dispersion coefficient of C_7H_8 (m^2/s) Axial mass dispersion coefficient of H_2O (m^2/s) Axial mass dispersion coefficient of H_2 (m^2/s) Axial mass dispersion coefficient of CO (m^2/s) Void fraction of bed (m^3gas/m^3reactor) Effectiveness factor (-)	0.1501 0.5892 $1.31x10^{-5}$ $1.06x10^{-8}$ $6.14x10^{-6}$ $2.97x10^{-5}$ $9.02x10^{-6}$ $2.01x10^{-5}$ 0.41 0.0139 (1250 K)

3.2. Temperature profiles and reactant and product distributions

A mathematical model is developed for simulating the heat and mass transfer processes coupled with thermochemical reaction kinetic in STR according to figures below.

Figure 2 shows the temperature profiles of the gas phase along SRT length with different inlet superficial velocity (V_{sg}). As it can be seen in Fig.2. five different V_{sg} (0.90 – 1.90 m/s) are used to check the effect of these V_{sg} on the temperature the temperature in the gas phase. The temperature profiles of the gas phase decreases from 1800 K as the V_{sg} as the increases. For example, the temperature profiles of the gas phase is of 1242.37 K when the V_{sg} is of 0.90 m/sec while it decreases to 1017.91 K when the V_{sg} increases to 1.90 m/s. Furthermore, the thermal equilibrium temperature on the gas outlet surface increases with the decrease of the V_{sg} to keep total energy conservation of the SRT process. As consequence, the increase of the V_{sg} can effectively decrease the temperature in the gas phase and temperature gradient which in turn can increase the safety of the fixed bed of the SRT.

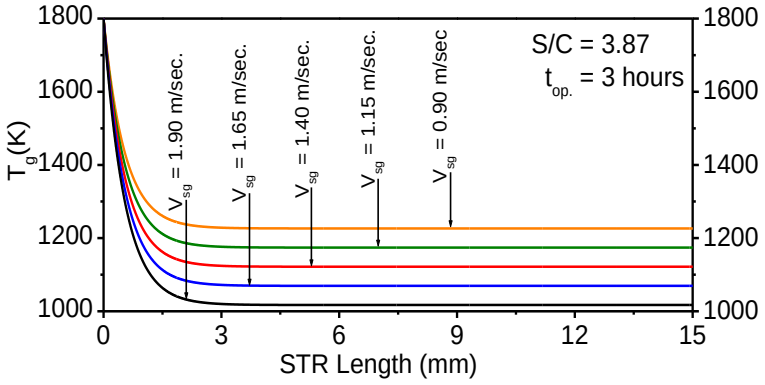

Figure 2: Comparisons of the temperature profiles of the gas phase along the STR length on Ni/γ-Aℓ_2O_3

Figure 3 reports the reactant and product distributions along the fixed bed of the porous medium SRT with radiative heat loss. As it was observed in this figure, the reactant mole concentration (C_7H_8 and H_2O) distributions decrease sharply along the fixed bed and then reactant mole concentration distributions have small fluctuation along the fixed bed up to the gas outlet surface. The mole concentration of H_2 increases remarkably at the near gas inlet surface region and reach its maximum value and then it follows constant until the gas outlet surface. On the other hand, the mole concentration of CO increases more slowly along the fixed bed and achieve its maximum values and so it follows constant up to the gas outlet surface

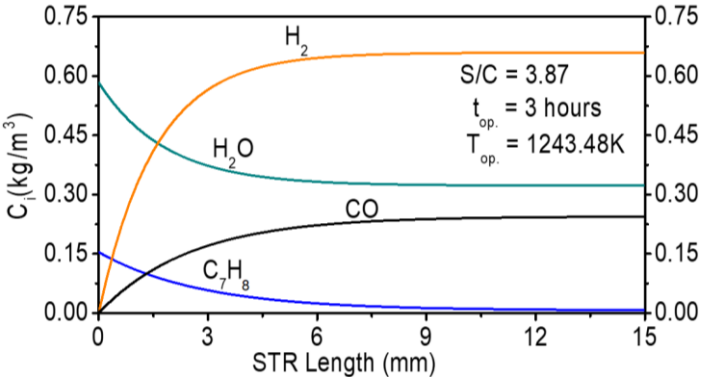

Figure 3: Reactant and product distributions along the STR length on Ni/γ-Aℓ$_2$O$_3$

3.3. Conversions of C_7H_8 and DRT of H_2 and CO

The SRT process can be characterized by the overall conversion of C_7H_8 on the model reaction. After reaching the stable levels of temperature and concentrations of reactants and products, the overall conversion of C_7H_8 can be computed by Eq. (6a) below.

$$Conver.\ of\ C_7H_8 = 1 - \frac{C_{C_7H_8}}{C_{C_7H_8,0}} \tag{6a}$$

Figure 4 shows the effect of the operating time on the overall conversion of C_7H_8 on the model reaction at operating conditions of 650 KPa and 1243.48 K along the fixed bed from SRT with radiative heat loss. Beyond that, results of the overall conversion of C_7H_8 on the model reaction were computed at five different operating times. From Fig. 4, the overall conversion of C_7H_8 is achieved to be at the center of outlet surface with the values of 0.0000 (t_1 = 0.00 hour), 0.5204 (t_2 = 1.0 hour), 0.6873 (t_3 = 1.5 hours), 0.8158 (t_4 = 2.0 hours), and 0.9467 (t_5 = 3.0 hours), respectively.

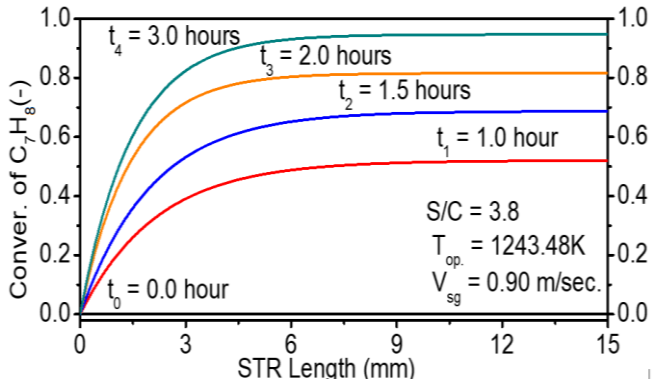

Figure 4: Effect of the operating time on conversions of C_7H_8 along the STR length of the SRT reaction on Ni/γ-Aℓ$_2$O$_3$ ($d_{p,av.}$ = 96μm) with 9% Ni loading

The dimensionless flow rate (DFR) of H_2 relative to initial concentration of C_7H_8 can be used as suitable me to compute the amount of H_2 in the SRT process. Thus, the calculation of this DFR is carried out by Eq. (6b) as follows.

$$DFR\ of\ H_2 = \frac{C_{H_2}}{C_{C_7H_8,0}} \tag{6b}$$

Figure 5 shows the effect of the operating temperature on the DFR of H_2 of SRT process with radiative heat loss. The DFR of H_2 increases with the increase the operating temperature due to endothermicity of the SRT reaction (Eq (1a)). As it can be seen in Fig.5, this fact leads to higher DFR of H_2 at higher operating temperature. A computer code to simulate and analyze the performance of the thermochemical process variables allowed the following conclusions.

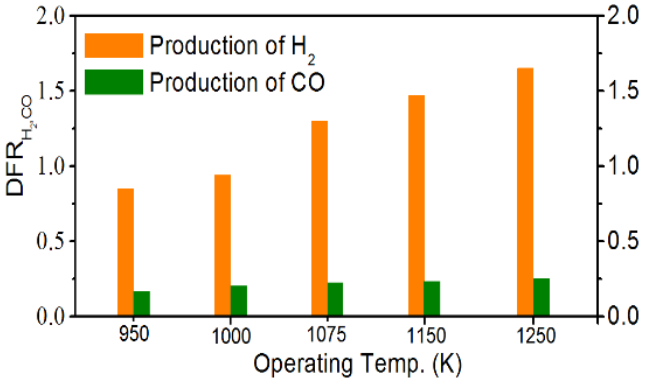

Figure 5: Effect of the operating temperature on the DRT of H_2 and CO of the SRT on Ni/γ-Aℓ_2O_3 *($d_{p,av.}$ = 96μm) with 9%* Ni *loading.*

4. CONCLUSIONS

The heat transfer and thermochemical performance of the SRT process are numerically investigated with radiative heat loss. A mathematical model was developed to simulate the heat and mass transport coupled with thermochemical reaction kinetic. For this purpose, the finite volume method was used to solve the mathematical model.

1. The temperature profiles of the gas phase are sharply affected by the Vsg. As results, reaction temperature at the outlet surface region from the STR has varied of 1017.19 < T_{react} < 1243.48 K.
2. The reactant (C_7H_8 and H_2O) distributions decrease sharply along the STR length while product (H_2 and CO) distributions increase remarkably along the STR length.
3. The overall conversion of C_7H_8 had reached a value of 94.58% at the operating time of 3.0 hours.
4. The DFR of products (H2 and CO) is remarkably increased with the operating temperature and its maximum values had reached 1.6521 and 0.2548 at 1250 K.

5. REFERENCES

Wang, F., Lin, J., Ziming, C., Huaxu, L., Jianyu, T., 2019. "Combination of thermodynamic analysis and regression analysis for steam and dry methane reforming". *International Journal of Hydrogen Energy*, Vol. 44, No. 30, pp. 15795-15810.

Chen, X.; Wang, F.; Han, Y.; Yu, R.; Cheng, Z., 2018. "Thermochemical storage analysis of the dry reforming of methane in foam solar reactor". *Energy Conversion and Management*, Vol. 158, pp. 489-498.

Leonzio, G., 2019. "ANOVA analysis of an integrated membrane reactor for hydrogen production by methane steam reforming". *International Journal of Hydrogen Energy*, Vol. 44, No. 23, pp. 11535-11545.

Ceylan, I., Gurel A.E., Ergun, A., 2017. "The mathematical modeling of concentrated photovoltaic module temperature". *International Journal of Hydrogen Energy*, Vol. 42, No. 31, pp. 19641-19653.

Cruz, B.M., Silva, J.D., 2017. "A two-dimensional mathematical model for the catalytic steam reforming of methane in both conventional fixed-bed and fixed-bed membrane reactors for the Production of hydrogen". *International Journal of Hydrogen Energy*, Vol. 42, pp. 23670-23690.

Silva, P.B.A., Carvalho, J.D.C.G., Silva, J.D., 2019. "Hydrogen adsorption on Ni/γ-Aℓ_2O_3 in a fixed-bed adsorber: Experimental validation and numerical modelling". *International Journal of Hydrogen Energy*, Vol. 44, pp. 304-317.

Silva, J.D.,2015. "Numerical modelling for a catalytic trickle-bed reactor using Laplace transform technique". *Chemical Engineering Transactions*, Vol. 43, pp. 1573-1578.

Teles, V.H.B, Silva, J.D., 2015. “Pressure swing adsorption technology using 5A zeolite for the removal of H_2S in the fixed bed reactor”. *Chemical Engineering Transactions*, Vol. 43, pp. 1111-1116.

Silva, J.D., Oliveira, C.B., 2012. “Fluidynamics modelling for a fixed bed gasifier using Laplace transform finite difference method”. *Procedia Engineering*. Vol. 42, pp. 753-769.

6. RESPONSIBILITY NOTICE

The authors are the only responsible for the printed material included in this paper.